Wall loss of semi-volatile organic compounds in a Teflon bag chamber for the temperature range of 262-298 K: mechanistic insight on temperature dependence

Longkun He[1], Wenli Liu[2], Yatai Li[1,3], Jixuan Wang[1], Mikinori Kuwata[2], Yingjun Liu[1]

[1]State Key Joint Laboratory of Environmental Simulation and Pollution Control, College of Environmental Sciences and Engineering, Peking University, Beijing, 100871, China
[2]Department of Atmospheric and Oceanic Sciences and Laboratory for Climate and Ocean-Atmosphere Studies, School of Physics, Peking University, Beijing 100871, China
[3]Now at College of Public Health, Zhengzhou University, Zhengzhou, 450001, China

Correspondence to: Mikinori Kuwata (kuwata@pku.edu.cn), Yingjun Liu (yingjun.liu@pku.edu.cn)

Abstract. Teflon bag chambers have long been used for investigating atmospheric chemical processes, including secondary organic aerosol formation. The wall-loss process of gas-phase species in Teflon bag chambers has typically been investigated at around room temperature. Recent laboratory studies started employing Teflon bag chambers at sub-273 K conditions for simulating wintertime and upper tropospheric environments. However, temperature dependence in vapor wall-loss processes of semi-volatile organic compounds (SVOCs) in a Teflon bag chamber has not well been investigated. In this study, we experimentally investigated wall-loss process of C_{14}-C_{19} *n*-alkanes in a 1 m^3 Teflon bag for the temperature range of 262 to 298 K. Enhanced wall losses of the tested *n*-alkanes were observed following the decrease in temperature. For instance, 65% of C_{14} *n*-alkane was lost to the wall 15 hours after injection at room temperature, while the corresponding value was 95% at 262 K. The experimental data were analyzed using the two-layer kinetic model, which considers both absorption of gas phase species to the surface layer of Teflon wall and diffusion to the inner layer. The experimental data demonstrated that absorption of gas phase species by the surface layer enhanced at lower temperature. The temperature dependence in absorption was well accounted using the equilibrium dissolution model of organic compounds to the Teflon surface by considering reduced saturation vapor pressure at lower temperature. On the contrary, diffusion of *n*-alkanes from the surface to inner layer slowed down at reduced temperature. Mechanistic studies on these processes will need to be conducted in the future to quantitatively predict the influence of temperature-dependent wall-loss processes of SVOCs on laboratory experimental results.

1 Introduction

The environmental chamber is one of the most widely-used laboratory systems for studying chemical processes in the atmosphere, including formation of secondary organic aerosol (SOA) (Clark et al., 2016; Nakao et al., 2011; Ng et al., 2007; Song et al., 2005). The environmental chambers are typically made of Teflon films or stainless steel (Cocker et al., 2001; Voigtlaeander et al., 2012). Existence of walls in the environmental chambers induces losses of both vapors and particles due to their deposition on wall surfaces (Mcmurry and Grosjean, 1985; Krechmer et al., 2020). Wall loss of gas-phase organic compounds in the environmental chambers can lead to underestimation of SOA mass yields. For instance, injection of seed particles into Teflon bag has been shown to increase SOA yields by a few times due to the reduced relative importance of the chamber wall as a condensation sink in the system (Kroll et al., 2007; Zhang et al., 2014).

Vapor wall loss in Teflon bag chambers, especially that for semi-volatile organic compounds (SVOCs), has been intensively investigated in the last decade (Matsunaga and Ziemann, 2010; Yeh and Ziemann, 2014, 2015; Zhang et al., 2015; Krechmer et al., 2016; Huang et al., 2018b; Pratap et al., 2020; Yu et al., 2022). For instance, Matsunaga and Ziemann (2010) studied wall-loss process of alkanes, alkenes, alcohols, and ketones. These previous wall-loss experiments were dominantly conducted at around room temperature (293~303 K), as most of the chamber studies employed the corresponding temperature range (Hidy, 2019). The experimental results were often modeled by assuming equilibrium dissolution of the organic compounds into the Teflon film. A more recent study separately considered the surface and inner layer of the Teflon film for explaining the loss process more quantitatively (Huang et al., 2018b).

Recently, a growing number of environmental chamber experiments have been conducted at low temperatures to simulate wintertime/upper tropospheric conditions in laboratory (Huang et al., 2018a; Pratap et al., 2019; Quelever et al., 2019; Simon et al., 2020; Wang et al., 2022). For instance, some SOA formation experiments have been conducted for the temperature range down to 223 K using stainless steel chambers such as the Aerosol Interaction and Dynamics in the Atmosphere (AIDA) and Cosmics Leaving OUtdoor Droplets (CLOUD) chambers (Huang et al., 2018a; Simon et al., 2020). Teflon bag chambers have also been employed for the temperature range down to 258 K (Kristensen et al., 2017; Deng et al., 2021). These studies demonstrate that temperature is an important parameter determining both mass yields and chemical composition of SOA. Vapor wall loss of SVOCs in the environmental chambers for the corresponding temperature range needs to be understood for better interpreting these experimental data in a quantitative way. So far only one group attempted to investigate vapor wall loss below room temperature, by measuring the size evolution of levoglucasan particles injected into a Teflon chamber (Pratap et al., 2020). However, the experimental results were confounded by slow evaporation of levoglucosan from particles at low temperatures.

This study investigated vapor wall loss of C_{14}-C_{19} *n*-alkanes in a Teflon chamber for the temperature range of 262 to 298 K by monitoring the evolution of their gas-phase concentrations following a pulse release. The wall-loss process was

investigated as a function of temperature. The experimental results were analyzed using the two-layer kinetic model, which considers partitioning of gas phase SVOCs to the surface layer, as well as further diffusion to the inner layer. Temperature effects on the two processes were evaluated separately.

2 Experimental

2.1 Teflon chamber experiments

Figure 1 shows the experimental setup. The experiment was conducted using a fluorinated ethylene propylene (FEP) bag with the volume of 1 m^3. The thickness of the FEP film for the bag was 75 μm. The dimension of the bag was 260 cm × 55 cm × 70 cm. The area to volume ratio of the chamber was 7.26 m^{-1}. The chamber volume was experimentally validated by employing CO_2 as a tracer (Figure S1). The timescale for CO_2 to be well mixed in the bag after a pulse injection was approximately 30 mins (Figure S1). The bag was newly purchased for the experiment, meaning that it was employed for no other experiments. The bag was installed in a chest freezer (Type 2288, Nixue Inc.), which was equipped with an additional internal thermal insulation layer. Two fans were installed in the freezer (outside the bag) to facilitate mixing of air so that air temperature in the freezer was uniform. The temperature of the freezer was measured at 3 points using temperature sensors (Figure 1). Temporal variation of temperature was ± 0.5 K at 262 K.

Throughout the experiments, purified air was employed. The purified air was produced using a zero air generator (Model 747−30, AADCO Instruments, Inc.) and further purified using a hydrocarbon trap (BHT-2, Agilent Technologies, Inc.). Hydrocarbon concentration in the purified air was less than 5 ppbv. Relative humidity (RH) was less than 0.1%.

Solutions containing C_{14} - C_{19} *n*-alkanes (Konoscience Inc., > 98%) were prepared and injected into the chamber. Hexane (Fisher Chemical Co., HPLC grade) was employed as the solvent. The purities and saturation vapor pressures of all chemicals are given in Table S1. The solutions were injected to the chamber using a syringe pump (Fusion 200 Touch, Chemyx Inc.) and a nebulizer (TR-30-A1, Meinhard Inc.) through polytetrafluoroethylene (PTFE) tubing, as shown in Figure 1. The use of nebulizer expedited the evaporation of the solution.

Eight sets of wall-loss experiments were conducted in the temperature range of 262 to 298 K. Prior to each experiment, the chamber was heated to ~320 K and continuously flushed using purified air. The cleaning process lasted for 2~3 days until the concentration of investigated *n*-alkanes dropped to the background level. To start an experiment, the chamber was switched to batch mode and the solution was injected to the chamber at room temperature. The injection lasted for 13 mins, with a liquid flow rate of 100 μL min^{-1}. The air flow rate of the nebulizer was 0.7 L min^{-1}. The resulting initial concentrations (C_0) of individual *n*-alkanes in the chamber ranged from 4 to 50 μg m^{-3} assuming no wall loss, which were lower than 20% of their saturation concentrations under the corresponding experimental temperature to avoid particle formation. The solution used for low-temperature experiments (< 278 K) did not contain C_{18} and C_{19} *n*-alkanes to avoid formation of particles. For experiments

below room temperature, the cooling system of the freezer was turned on one hour after the completion of the injection. The operation procedure was employed to avoid homogeneous nucleation and subsequent condensational growth of aerosol particles. The validity of employing this post-cooled operation procedure was demonstrated by comparison with a pre-cooled chamber result at 270 K (Figure S2). Measurements using an optical particle counter (11-D, GRIMM Aerosol Technik Ainring, Germany) experimentally confirmed negligible abundance of aerosol particles in the chamber (< 0.5 μg m^{-3}). It took ~3 hours for the temperature in the freezer to drop to a stable level after injection (Figure S3). Although the air in the bag leaked out during experiments due to compression of the bag by its own weight, absence of intrusion of room air to the bag was confirmed by observing no changes in contaminant signals (Table S2). The gas-phase concentrations of *n*-alkanes were therefore unaffected by the changes in bag volume.

Concentrations of SVOCs in the chamber were quantified using the semi-volatile thermal desorption aerosol gas chromatograph (SV-TAG, Aerodyne Research Inc. & Aerosol Dynamic Inc., USA) (Zhao et al., 2013). The gas chromatography-mass spectrometer (GC-MS) (7890B, Agilent Technologies, Inc.) was employed for the system. Detailed descriptions of the SV-TAG operation and performance tests were presented in our previous papers (Li et al., 2022a; Li et al., 2022b). Herein, chamber air was sampled through ~1 m long perfluoroalkoxy alkane (PFA) tubing (1/4 inch in diameter). Prior to sampling, the chamber air passed through the PFA tubing at 0.5 L min^{-1} for at least 20 min for passivating the tubing wall (Matsunaga and Ziemann, 2010). Samples were periodically collected for 5 min at 4 L min^{-1} for each time at 1-15 hours after injection. As the absence of particles was confirmed, only gas-phase SVOCs were sampled by the SV-TAG. The instrument response to *n*-alkanes was calibrated with standards before and after each experiment (Figure S4), utilizing the in-situ automatic injection system (Isaacman et al., 2011). The gas-phase concentrations of SVOCs were calculated from the measured quantity of SVOCs and sampled air volume.

2.2 Kinetic model

Herein we used a unified vapor wall-loss transport model developed by Huang et al. (2018b) to fit the experimental data. Figure 2 shows the concept of the model. Briefly, SVOCs partition between the gas phase and the surface of the FEP film. Subsequently, the absorbed SVOCs may diffuse to the inner layer of the film. As the thickness of the FEP film (75 μm) is a couple of orders larger than that of the surface layer (~ 5 nm) (Huang et al., 2018b), the inner layer is assumed as an infinite sink. As a result, the diffusion process of SVOCs from the inner layer to the film surface is ignored. A list of all the parameters is provided in Nomenclature. The governing equations without and with considering diffusion to the inner layer are presented below, respectively.

(1) Without considering the diffusion process in the inner layer, the wall loss process is solely controlled by partitioning of SVOCs between the gas phase and surface layer and can be described as follows

$$\text{Gas phase} \underset{k_{-1}}{\overset{k_1}{\rightleftharpoons}} \text{Surface} \quad (1)$$

where k_1 and k_{-1} are forward and backward rate constants in the process. The corresponding first-order kinetic equations are

$$\begin{aligned} \frac{dC_{gas}}{dt} &= -k_1 C_{gas} + k_{-1} C_{surface} \\ \frac{dC_{surface}}{dt} &= k_1 C_{gas} - k_{-1} C_{surface} \end{aligned} \quad (2)$$

where C_{gas} and $C_{surface}$ are the SVOC concentrations in gas phase and on wall surface, respectively. It should be noted that $C_{surface}$ was defined as the total mass of SVOC on wall surface divided by the chamber volume, following previous studies (Matsunaga and Ziemann, 2010; Yeh and Ziemann, 2014, 2015). This model has been commonly used to interpret the experimental data of vapor wall loss in previous studies (Matsunaga and Ziemann, 2010; Yeh and Ziemann, 2014, 2015; Zhang et al., 2015).

The gas-surface equilibrium time scale $\tau_{surface}$ and equilibrium constant K_{eq} can be obtained by

$$\tau_{surface} = \frac{1}{k_1 + k_{-1}} \quad (3)$$

$$K_{eq} = \frac{k_1}{k_{-1}} = \left[\frac{C_{surface}}{C_{gas}}\right]_{eq} \quad (4)$$

(2) Considering the diffusion process in the inner layer, the whole vapor wall loss process can be formulated as follows

$$\text{Gas phase} \underset{k_{-1}}{\overset{k_1}{\rightleftharpoons}} \text{Surface} \overset{k_2}{\rightarrow} \text{Inner Layer} \quad (5)$$

where k_2 is the first-order loss rate constant in the diffusion process. Correspondingly, the kinetic processes for C_{gas} and $C_{surface}$ can be described by the following equations

$$\begin{aligned} \frac{dC_{gas}}{dt} &= -k_1 C_{gas} + k_{-1} C_{surface} \\ \frac{dC_{surface}}{dt} &= k_1 C_{gas} - k_{-1} C_{surface} - k_2 C_{surface} \end{aligned} \quad (6)$$

The diffusion process has the first-order decay time scale τ_{inner} of $\tau_{inner} = \frac{1}{k_2}$. If $k_2 \ll k_1 + k_{-1}$ (*i.e.*, $\tau_{inner} \gg \tau_{surface}$), gas-surface partitioning occurs much faster than the diffusion process to the inner layer. In this case, the apparent first-order decay loss constant of SVOC from the gas phase can asymptotically be represented as (Huang et al., 2018b):

$$\frac{dC_{gas}}{C_{gas}dt} \approx -\frac{K_{eq}}{1+K_{eq}}k_2 \quad (7)$$

The data analysis and model fitting were conducted using Wolfram Mathematica 13.1. The controlling factors of individual parameters in the above equations were previously discussed by Huang et al. (2018b).

3 Results and discussion

3.1 Wall loss of *n*-alkanes at room temperature

An example of temporal profile for C_{14}-C_{19} *n*-alkanes during the experiment at 298 K is shown in Figure 3. The figure demonstrates the temporal change of C_{gas}/C_0, where C_0 indicates the initial concentration of *n*-alkanes. The values of C_{gas}/C_0 for each *n*-alkane exhibited similar temporal patterns. During the first one hour following the injection, C_{gas}/C_0 exponentially decreased. After that, gradual decreases in C_{gas}/C_0 were observed. For example, the decline in gas fraction for C_{14} *n*-alkane during the first hour accounted for 71% of the total change in C_{gas}/C_0 over the whole experimental period of 15 hours. The values of C_{gas}/C_0 decreased with the increase in carbon number, indicating enhanced wall loss. The values of C_{gas}/C_0 at 15 hours after injection were 0.32, 0.25, 0.16, 0.097, 0.069, and 0.037 for C_{14} - C_{19} *n*-alkanes, respectively.

The experimental result can be well fitted using the two-layer model, but the fits deteriorate in the case that diffusion in the inner layer is neglected (Figure 3). The optimized parameter sets are shown in Table S3. Mass fractions of injected chemical species in the gas, surface, and inner layer phases that were estimated using the model are shown in Figure S5. In the case of the most volatile compound (C_{14} *n*-alkane), the maximum mass fraction in the surface phase occurred at 2 hours after injection. Subsequently, the mass fractions for the compound in both gas phase and surface layer gradually decreased. During this period, the ratio of the mass in the surface layer to that in the gas phase stabilized at 1.33. The mass fraction of the compound in the inner layer steadily increased, reaching 0.22 at 15 hours after injection.

In the case of the least volatile compound (C_{19} *n*-alkane), the mass fraction in the surface layer reached the maximum (~76%) approximately 1 hour after injection, accounting for the rapid decrease in the observed concentration in the gas phase. Subsequently, mass fractions of the compound in the gas phase and in the surface layer decreased in proportion. The concentration ratio of the gas phase and surface layer stayed constant (Figure S5). The mass fraction of the compound in the inner layer kept increasing during the experiment. At 15 hours after injection, 87% of the compound existed in the inner layer.

The time scale for *n*-alkanes to reach partitioning equilibrium between the gas and surface phases is estimated to be 12 ~ 35 mins, consistent with literature data. For example, Matsunaga and Ziemann (2010) reported that the corresponding time scale for C_8 - C_{16} alkanes was 60 ± 20 mins. The corresponding value for oxygenated organic compounds was reported as 26 ± 23 mins (Yeh and Ziemann, 2015).

Our result for the mass transfer of SVOCs to the inner layer can also be compared with a previous study. The rates for the decrease in C_{gas}/C_0 for C_{14}-C_{19} *n*-alkanes were 0.6–1.3% hour^{-1} after the partitioning between gas phase and surface layer reached equilibrium (*i.e.*, 3 ~ 15 hours). Yeh and Ziemann (2015) reported the corresponding value for 2-ketones as approximately 1% hour^{-1} for the time scale of 7 hours. They suggested that the value is close to the theoretical value for the Fickian diffusion loss rate (~0.5 % hour^{-1}).

3.2 Temperature dependence of wall loss of *n*-alkanes

Figure 4a summarizes the values of C_{gas}/C_0 for all experiments at 3 hours after injection. The data for this sampling time were selected, as the loss of gas phase species by partitioning to the surface layer accounted for the dominant portion of the decline in the gas phase concentration. Generally, C_{gas}/C_0 was lower for less volatile compounds and at lower temperature, suggesting enhanced partitioning of *n*-alkanes to the chamber wall. The data for the room temperature (C_{gas}/C_0 = 0.47, 0.45, 0.34, 0.24, 0.17, and 0.091 for C_{14}, C_{15}, C_{16}, C_{17}, C_{18}, and C_{19} *n*-alkanes) were smaller than that have been reported by a previous study. Namely, Matsunaga and Ziemann (2010) quantified the corresponding values for equilibration between the gas and surface phases for C_{14}-C_{16} *n*-alkanes as ~80 – 90%. The enhanced partitioning to the surface layer in our study is likely due to that the chamber for the present study has a larger area to volume ratio (7.26 m^{-1} versus 3.39 m^{-1}).

Figure 4b shows the values of C_{gas}/C_0 as a function of temperature at 15 hours after injection. In all experiments, the values of C_{gas}/C_0 at 15 hours after injection were consistently lower than those for 3 hours. For instance, C_{gas}/C_0 for C_{14} *n*-alkane at 262 K decreased from 0.15 (3 hours) to 0.06 (15 hours). As discussed in the case of the experiment at 298 K, the result suggests that diffusional loss in the inner layer of the chamber wall occurred for the whole temperature range.

3.3 Temperature dependence of partitioning between gas phase and wall surface

The temperature dependence in the data summarized in Figure 4a can be understood by considering changes in partitioning between the gas phase and surface layer. Matsunaga and Ziemann (2010) introduced the following equation for relating $C_{surface}/C_{gas}$ and temperature based on the equilibrium dissolution model:

$$\left[\frac{C_{surface}}{C_{gas}}\right]_{eq} = K_{eq} = \frac{C_{FEP\_surface}RT}{M_{wall}\gamma_{FEP\_surface}P_s(T)} \quad (8)$$

where $C_{FEP\_surface}$ is the equivalent organic mass concentration of the FEP chamber surface wall, M_{wall} is the average molecular mass of the FEP, $\gamma_{FEP\_surface}$ is the activity coefficient of the organic compound in the Teflon surface, R is the gas constant, and T is temperature. $P_s(T)$ is the saturation vapor pressure of the compound at temperature T. Among the terms for the right-hand-side of equation (8), $RT/P_s(T)$ can be calculated from the experimental conditions. Herein $P_s(T)$ was calculated by the EVAPORATION group contribution method (Compernolle et al., 2011). Comparison between the EVAPORATION method and other approaches for estimating $P_s(T)$ is available in Figure S6. The equation suggests that $[C_{surface}/C_{gas}]_{eq}$ and $RT/P_s(T)$ may vary in proportion, with the slope of $C_{FEP\_surface}/(M_{wall}\gamma_{FEP\_surface})$.

It is challenging to retrieve the value of $[C_{surface}/C_{gas}]_{eq}$ by fitting the data of the low-temperature experiments using the two-layer model, since the chamber was cooled after the injection of *n*-alkanes. Alternatively, the value of $[C_{surface}/C_{gas}]_{eq}$ was approximated using $1/[C_{gas}/C_0]_{\text{at 3 hours}} - 1$, assuming that diffusion of *n*-alkanes to the inner layer was still a minor loss process within 3 hours. Potential uncertainties associated with this approximation are summarized in Text S1. The uncertainties were estimated in two ways: (1) kinetic simulation based on fitting parameters in Figure 3 (Figure S5) and (2) comparison of the retrieved values of $[C_{surface}/C_{gas}]_{eq}$ (*i.e.*, K_{eq}) and $1/[C_{gas}/C_0]_{\text{at 3 hours}} - 1$ at room temperature (Table S3). The room-temperature experiments were conducted for three runs, allowing for the estimation of experimental uncertainties as standard deviation. Although the kinetic simulation implies overestimates of 7 - 55%, the measurement-based comparison demonstrates that $1/[C_{gas}/C_0]_{\text{at 3 hours}} - 1$ and $[C_{surface}/C_{gas}]_{eq}$ agree within the experimental uncertainties, thereby supporting the validity of the approximation.

Figure 5 shows the correlations between $C_{surface}/C_{gas}$ and $RT/P_s(T)$ for individual compounds. For all the tested compounds, these two parameters correlated well, even though $C_{surface}/C_{gas}$ increased by more than one order of magnitude when the chamber was cooled down. The result suggests that equation (8) can be applied to a wide range of temperatures without considering the temperature dependence of $C_{FEP\_surface}/(M_{wall}\gamma_{FEP\_surface})$. In other word, $\gamma_{FEP\_surface}$ can be practically treated as a constant for the investigated temperature range, given $C_{FEP\_surface}$ and M_{wall} are independent of temperature. This implication is consistent with previous findings that the activity coefficients of organic compounds in polymers only change slightly with temperature. For instance, Kontogeorgis et al. (1993) compared the experimental and modelled values of activity coefficients for hydrocarbons in a few polymers such as low-density polyethylene. The values of activity coefficients change by 10~20% for a temperature change of 100 K.

Values of $\gamma_{FEP\_surface}$ for *n*-alkanes can be estimated from Figure 5. Based on equation (8), the fitted slopes correspond to $C_{FEP\_surface}/(M_{wall}\gamma_{FEP\_surface})$. For a specific chamber design, compound-independent $C_{FEP\_surface}$ can be estimated by the density of FEP film (2150 kg m^{-3}) ,the thickness of surface layer (~ 5 nm), and the surface-to-volume ratio of

the chamber (Huang et al., 2018b).The estimated $C_{FEP\_surface}$ for the chamber in this experiment was 78.2 mg m^{-3}. For estimating compound-dependent $\gamma_{FEP\_surface}$, previous studies assumed M_{wall} = 200 g mol^{-1} (Huang et al., 2018b; Matsunaga and Ziemann, 2010). The same approximations were employed in the present study.

Figure 6 plots the retrieved values of $\gamma_{FEP\_surface}$ for *n*-alkanes against $P_s(298\ \mathrm{K})$ for *n*-alkanes. The figure also shows the corresponding parameters obtained from previous experimental studies (compiled by Huang et al. (2018b), including Matsunaga and Ziemann (2010), Yeh and Ziemann (2014, 2015), and Krechmer et al. (2016)). It should be noted that the literature results were analyzed with fixed values of area to volume ratio of 3 m^{-1} and $C_{FEP\_surface}$ of 32.2 mg m^{-3} (Huang et al., 2018b). Regardless of differences in types of chemicals and chambers, the experimentally estimated values of $\gamma_{FEP\_surface}$ and $P_s(298\ \mathrm{K})$ correlate in logarithmic scale. The relationship followed the equation of $\ln(\gamma_{FEP_{surface}}) = 0.40 - 0.61\ln(P_s(298\ \mathrm{K}))$.

3.4 Characterization of diffusion from the Teflon surface to inner layer

Values of k_2 were estimated using equation (7), since values of τ_{inner} are at least 18 times larger than those of $\tau_{surface}$ (Table S3). The values of C_{gas}/C_0 at 3 hours after injection were employed to calculate K_{eq} as discussed earlier. The experimental data for 9, 12, and 15 hours after injection was employed for obtaining k_2.

Figure 7 plots the estimated values of k_2 against $P_s(T)$ for all compounds in all experiments. The values of k_2 and $P_s(T)$ positively correlate. As a comparison point, a previous study reported positive correlations for (1) the diffusivity of organic compounds in FEP film and saturation concentration, and (2) k_2 and diffusivity (Huang et al., 2018b). Our current result is qualitatively similar to the previous study, though temperature was maintained as a constant in the previous study. The decrease in k_2 at lower temperature could be induced by reduced viscosity in the inner layer or weakened thermal motion of *n*-alkane molecules (Mattila et al., 2023). It should be noted that compression of bag volume during experiment would lead to an increase in the area to volume ratio. Consequently, this could disrupt the relatively slow diffusion process. Based on some photos during the experiment, the leak-out air could have increased the area to volume ratio by a few times. Further study, that considers changes of chamber volume, would be needed in the future for quantitatively interpreting the data.

4 Conclusions

The present study investigated the wall loss process of C_{14}-C_{19} *n*-alkanes to the wall of a 1 m^3 chamber bag, which was composed of FEP film. The temperature of the chamber was controlled for the range of 262 to 298 K. Decay in gas-phase concentrations of the *n*-alkanes was quantified using the SV-TAG for 15 hours following injection. The temporal variations in the *n*-alkane concentrations suggested two types of loss processes. The first process was characterized by rapid exponential

decay in the first few hours. Subsequently, slow first-order decrease in the *n*-alkane concentrations was identified until the end of the experiment. Enhanced wall loss was observed at lower temperatures for all compounds.

The experimental data were well fitted using the two-layer kinetic model, which considers partitioning of gas-phase species to the surface layer of the chamber film and further diffusion to the inner layer. The analysis suggests that when the Teflon bag chamber is operated at low temperatures, partitioning of gas phase species to the chamber wall surface is enhanced, whereas the permeation of the chemical compounds to the inner layer is suppressed. The temperature effect on gas-surface partitioning overweighs that on diffusion into the inner layer for *n*-alkanes, leading to an overall enhanced wall loss at lower temperature.

The quasi-equilibrium partitioning of *n*-alkanes between the gas phase and surface layer was interpreted by considering the dissolution process of the species into the surface layer. Values of $C_{surface}/C_{gas}$ at quasi-equilibrium are proportional to $RT/P_s(T)$ for individual compounds. The result suggests that decreased saturation vapor pressure is the major driving force for enhanced partitioning to the surface layer at low temperatures for all investigated compounds, while their activity coefficients can be practically treated as constants for the investigated temperature range. The relationship can be potentially employed for predicting changes in wall loss of SVOCs as a function of temperature, after further verification employing other types of organic compounds.

In the future, the underlying mechanisms of the present findings will need to be sought for a better understanding of the chamber wall loss of SVOCs. The present study focused on *n*-alkanes. In the case of chamber experiments for SOA formation, wall loss processes of oxygenated chemical species would be more important. Thus, a temperature-dependent wall loss study for oxygenated chemical species will still need to be conducted for interpreting SOA chamber experiments under a wide range of temperatures.

Data Availability

Data will be made available on request.

Author contribution

Longkun He: Conceptualization, Methodology, Experiment, Data curation, Formal analysis, Writing – original draft. **Wenli Liu:** Methodology, Experiment, Writing – review & editing. **Yatai Li:** Methodology, Writing – review & editing. **Jixuan Wang:** Experiment, Writing – review & editing. **Mikinori Kuwata:** Conceptualization, Methodology, Project administration, Funding acquisition, Formal analysis, Writing – review & editing, Supervision. **Yingjun Liu:** Conceptualization, Methodology, Project administration, Funding acquisition, Formal analysis, Writing – review & editing, Supervision.

Competing interests

The authors declare that they have no conflict of interest.

Acknowledgements

We thank Dr. Ying Zhou for assisting to improve figure quality. This research was supported by the National Natural Science Foundation of China (92044303, 42175121, and 42150610485).

Reference

Clark, C. H., Kacarab, M., Nakao, S., Asa-Awuku, A., Sato, K., and Cocker, D. R., III: Temperature effects on secondary organic aerosol (SOA) from the dark ozonolysis and photo-oxidation of isoprene, Environ. Sci. Technol., 50, 5564-5571, https://doi.org/10.1021/acs.est.5b05524, 2016.

Cocker, D. R., Flagan, R. C., and Seinfeld, J. H.: State-of-the-art chamber facility for studying atmospheric aerosol chemistry, Environ. Sci. Technol., 35, 2594-2601, https://doi.org/10.1021/es0019169, 2001.

Compernolle, S., Ceulemans, K., and Muller, J. F.: EVAPORATION: A new vapour pressure estimation method for organic molecules including non-additivity and intramolecular interactions, Atmos. Chem. Phys., 11, 9431-9450, https://doi.org/10.5194/acp-11-9431-2011, 2011.

Deng, Y. G., Inomata, S., Sato, K., Ramasamy, S., Morino, Y., Enami, S., and Tanimoto, H.: Temperature and acidity dependence of secondary organic aerosol formation from alpha-pinene ozonolysis with a compact chamber system, Atmos. Chem. Phys., 21, 5983-6003, https://doi.org/10.5194/acp-21-5983-2021, 2021.

Hidy, G. M.: Atmospheric chemistry in a box or a bag, Atmosphere, 10, 401, https://doi.org/10.3390/atmos10070401, 2019.

Huang, W., Saathoff, H., Pajunoja, A., Shen, X. L., Naumann, K. H., Wagner, R., Virtanen, A., Leisner, T., and Mohr, C.: Alpha-pinene secondary organic aerosol at low temperature: Chemical composition and implications for particle viscosity, Atmos. Chem. Phys., 18, 2883-2898, https://doi.org/10.5194/acp-18-2883-2018, 2018a.

Huang, Y. L., Zhao, R., Charan, S. M., Kenseth, C. M., Zhang, X., and Seinfeld, J. H.: Unified theory of vapor-wall mass transport in Teflon-walled environmental chambers, Environ. Sci. Technol., 52, 2134-2142, https://doi.org/10.1021/acs.est.7b05575, 2018b.

Isaacman, G., Kreisberg, N. M., Worton, D. R., Hering, S. V., and Goldstein, A. H.: A versatile and reproducible automatic injection system for liquid standard introduction: Application to in-situ calibration, Atmos. Meas. Tech., 4, 1937-1942, https://doi.org/10.5194/amt-4-1937-2011, 2011.

Kontogeorgis, G. M., Fredenslund, A., and Tassios, D. P.: Simple activity-coefficient model for the prediction of solvent activities in polymer-solutions, Ind. Eng. Chem. Res., 32, 362-372, https://doi.org/10.1021/ie00014a013, 1993.

Krechmer, J. E., Day, D. A., and Jimenez, J. L.: Always lost but never forgotten: Gas-phase wall losses are important in all Teflon environmental chambers, Environ. Sci. Technol., 54, 12890-12897, https://doi.org/10.1021/acs.est.0c03381, 2020.

Krechmer, J. E., Pagonis, D., Ziemann, P. J., and Jimenez, J. L.: Quantification of gas-wall partitioning in Teflon environmental chambers using rapid bursts of low-volatility oxidized species generated in situ, Environ. Sci. Technol., 50, 5757-5765, https://doi.org/10.1021/acs.est.6b00606, 2016.

Kristensen, K., Jensen, L. N., Glasius, M., and Bilde, M.: The effect of sub-zero temperature on the formation and composition of secondary organic aerosol from ozonolysis of alpha-pinene, Environ. Sci.-Proc. Imp., 19, 1220-1234, https://doi.org/10.1039/c7em00231a, 2017.

Kroll, J. H., Chan, A. W. H., Ng, N. L., Flagan, R. C., and Seinfeld, J. H.: Reactions of semivolatile organics and their effects on secondary organic aerosol formation, Environ. Sci. Technol., 41, 3545-3550, https://doi.org/10.1021/es062059x, 2007.

Li, Y. T., He, L. K., Xie, D., Zhao, A. Q., Wang, L. X., Kreisberg, N. M., Jayne, J., and Liu, Y. J.: Strong temperature influence and indiscernible ventilation effect on dynamics of some semivolatile organic compounds in the indoor air of an office, Environ. Int., 165, 107305, https://doi.org/10.1016/j.envint.2022.107305, 2022a.

Li, Y. T., Xie, D., He, L. K., Zhao, A. Q., Wang, L. X., Kreisberg, N. M., Jayne, J., and Liu, Y. J.: Dynamics of di-2-ethylhexyl phthalate (DEHP) in the indoor air of an office, Build. Environ., 223, 109446, https://doi.org/10.1016/j.buildenv.2022.109446, 2022b.

Matsunaga, A. and Ziemann, P. J.: Gas-wall partitioning of organic compounds in a Teflon film chamber and potential effects on reaction product and aerosol yield measurements, Aerosol Sci. Technol., 44, 881-892, https://doi.org/10.1080/02786826.2010.501044, 2010.

Mattila, J. M., Li, E. Y., and Offenberg, J. H.: Tubing material considerably affects measurement delays of gas-phase oxygenated per- and polyfluoroalkyl substances, J. Air Waste Manage. Assoc., 73, 335-344, https://doi.org/10.1080/10962247.2023.2174612, 2023.

McMurry, P. H. and Grosjean, D.: Gas and aerosol wall losses in Teflon film smog chambers, Environ. Sci. Technol., 19, 1176-1182, https://doi.org/10.1021/es00142a006, 1985.

Nakao, S., Shrivastava, M., Anh, N., Jung, H., and Cocker, D., III: Interpretation of secondary organic aerosol formation from diesel exhaust photooxidation in an environmental chamber, Aerosol Sci. Technol., 45, 964-972, https://doi.org/10.1080/02786826.2011.573510, 2011.

Ng, N. L., Chhabra, P. S., Chan, A. W. H., Surratt, J. D., Kroll, J. H., Kwan, A. J., McCabe, D. C., Wennberg, P. O., Sorooshian, A., Murphy, S. M., Dalleska, N. F., Flagan, R. C., and Seinfeld, J. H.: Effect of NO_x level on secondary organic aerosol (SOA) formation from the photooxidation of terpenes, Atmos. Chem. Phys., 7, 5159-5174, https://doi.org/10.5194/acp-7-5159-2007, 2007.

Pratap, V., Bian, Q. J., Kiran, S. A., Hopke, P. K., Pierce, J. R., and Nakao, S.: Investigation of levoglucosan decay in wood smoke smog-chamber experiments: The importance of aerosol loading, temperature, and vapor wall losses in interpreting results, Atmos. Environ., 199, 224-232, https://doi.org/10.1016/j.atmosenv.2018.11.020, 2019.

Pratap, V., Kiran, S. A., Bian, Q., Pierce, J. R., Hopke, P. K., and Nakao, S.: Observation of vapor wall deposition in a smog chamber using size evolution of pure organic particles, Aerosol Air Qual. Res., 20, 2705-2714, https://doi.org/10.4209/aaqr.2020.05.0268, 2020.

Quelever, L. L. J., Kristensen, K., Jensen, L. N., Rosati, B., Teiwes, R., Daellenbach, K. R., Perakyla, O., Roldin, P., Bossi, R., Pedersen, H. B., Glasius, M., Bilde, M., and Ehn, M.: Effect of temperature on the formation of highly oxygenated organic molecules (HOMs) from alpha-pinene ozonolysis, Atmos. Chem. Phys., 19, 7609-7625, https://doi.org/10.5194/acp-19-7609-2019, 2019.

Simon, M., Dada, L., Heinritzi, M., Scholz, W., Stolzenburg, D., Fischer, L., Wagner, A. C., Kurten, A., Rorup, B., He, X. C., Almeida, J., Baalbaki, R., Baccarini, A., Bauer, P. S., Beck, L., Bergen, A., Bianchi, F., Brakling, S., Brilke, S., Caudillo, L., Chen, D. X., Chu, B. W., Dias, A., Draper, D. C., Duplissy, J., El-Haddad, I., Finkenzeller, H., Frege, C., Gonzalez-Carracedo, L., Gordon, H., Granzin, M., Hakala, J., Hofbauer, V., Hoyle, C. R., Kim, C., Kong, W. M., Lamkaddam, H., Lee, C. P., Lehtipalo, K., Leiminger, M., Mai, H. J., Manninen, H. E., Marie, G., Marten, R., Mentler, B., Molteni, U., Nichman, L., Nie, W., Ojdanic, A., Onnela, A., Partoll, E., Petaja, T., Pfeifer, J., Philippov, M., Quelever, L. L. J., Ranjithkumar, A., Rissanen, M. P., Schallhart, S., Schobesberger, S., Schuchmann, S., Shen, J. L., Sipila, M., Steiner, G., Stozhkov, Y., Tauber, C., Tham, Y. J., Tome, A. R., Vazquez-Pufleau, M., Vogel, A. L., Wagner, R., Wang, M. Y., Wang, D. S., Wang, Y. H., Weber, S. K., Wu, Y. S., Xiao, M., Yan, C., Ye, P. L., Ye, Q., Zauner-Wieczorek, M., Zhou, X. Q., Baltensperger, U., Dommen, J., Flagan, R. C., Hansel, A., Kulmala, M., Volkamer, R., Winkler, P. M., Worsnop, D. R., Donahue, N. M., Kirkby, J., and Curtius, J.: Molecular understanding of new-particle formation from alpha-pinene between -50 and +25 °C, Atmos. Chem. Phys., 20, 9183-9207, https://doi.org/10.5194/acp-20-9183-2020, 2020.

Song, C., Na, K. S., and Cocker, D. R.: Impact of the hydrocarbon to NO_x ratio on secondary organic aerosol formation, Environ. Sci. Technol., 39, 3143-3149, https://doi.org/10.1021/es0493244, 2005.

Voigtlaeander, J., Duplissy, J., Rondo, L., Kuerten, A., and Stratmann, F.: Numerical simulations of mixing conditions and aerosol dynamics in the CERN CLOUD chamber, Atmos. Chem. Phys., 12, 2205-2214, https://doi.org/10.5194/acp-12-2205-2012, 2012.

Wang, M. Y., Xiao, M., Bertozzi, B., Marie, G., Rorup, B., Schulze, B., Bardakov, R., He, X. C., Shen, J. L., Scholz, W., Marten, R., Dada, L., Baalbaki, R., Lopez, B., Lamkaddam, H., Manninen, H. E., Amorim, A., Ataei, F., Bogert, P., Brasseur, Z., Caudillo, L., De Menezes, L. P., Duplissy, J., Ekman, A. M. L., Finkenzeller, H., Carracedo, L. G., Granzin, M., Guida, R., Heinritzi, M., Hofbauer, V., Hohler, K., Korhonen, K., Krechmer, J. E., Kurten, A., Lehtipalo, K., Mahfouz, N. G. A., Makhmutov, V., Massabo, D., Mathot, S., Mauldin, R. L., Mentler, B., Muller, T., Onnela, A., Petaja, T., Philippov, M., Piedehierro, A. A., Pozzer, A., Ranjithkumar, A., Schervish, M., Schobesberger, S., Simon, M., Stozhkov, Y., Tome, A., Umo, N. S., Vogel, F., Wagner, R., Wang, D. S., Weber, S. K., Welti, A., Wu, Y. S., Zauner-Wieczorek, M., Sipila, M., Winkler, P. M., Hansel, A., Baltensperger, U., Kulmala, M., Flagan, R. C., Curtius, J., Riipinen, I., Gordon, H., Lelieveld, J., El-Haddad, I., Volkamer, R., Worsnop, D. R., Christoudias, T., Kirkby, J., Mohler, O., and Donahue, N. M.: Synergistic HNO_3-H_2SO_4-NH_3 upper tropospheric particle formation, Nature, 605, 483-489, https://doi.org/10.1038/s41586-022-04605-4, 2022.

Yeh, G. K. and Ziemann, P. J.: Alkyl nitrate formation from the reactions of C_8-C_{14} n-alkanes with OH radicals in the presence of NO_x: Measured yields with essential corrections for gas-wall partitioning, J. Phys. Chem. A, 118, 8147-8157, https://doi.org/10.1021/jp500631v, 2014.

Yeh, G. K. and Ziemann, P. J.: Gas-wall partitioning of oxygenated organic compounds: Measurements, structure-activity relationships, and correlation with gas chromatographic retention factor, Aerosol Sci. Technol., 49, 726-737, https://doi.org/10.1080/02786826.2015.1068427, 2015.

Yu, S., Jia, L., Xu, Y., Zhang, H., Zhang, Q., and Pan, Y.: Wall losses of oxygenated volatile organic compounds from oxidation of toluene: Effects of chamber volume and relative humidity, J. Environ. Sci., 114, 475-484, https://doi.org/10.1016/j.jes.2021.09.026, 2022.

Zhang, X., Cappa, C. D., Jathar, S. H., McVay, R. C., Ensberg, J. J., Kleeman, M. J., and Seinfeld, J. H.: Influence of vapor wall loss in laboratory chambers on yields of secondary organic aerosol, Proc. Natl. Acad. Sci. U. S. A., 111, 5802-5807, https://doi.org/10.1073/pnas.1404727111, 2014.

Zhang, X., Schwantes, R. H., McVay, R. C., Lignell, H., Coggon, M. M., Flagan, R. C., and Seinfeld, J. H.: Vapor wall deposition in Teflon chambers, Atmos. Chem. Phys., 15, 4197-4214, https://doi.org/10.5194/acp-15-4197-2015, 2015.

Zhao, Y. L., Kreisberg, N. M., Worton, D. R., Teng, A. P., Hering, S. V., and Goldstein, A. H.: Development of an in situ thermal desorption gas chromatography instrument for quantifying atmospheric semi-volatile organic compounds, Aerosol Sci. Technol., 47, 258-266, https://doi.org/10.1080/02786826.2012.747673, 2013.

Nomenclature

A table that contains the definitions of parameters and corresponding units.

k_1	forward rate constant (s^{-1})
k_{-1}	backward rate constant (s^{-1})
k_2	first-order loss rate constant (s^{-1})
$\tau_{surface}$	gas-surface equilibrium time scale (min)
τ_{inner}	diffusion time scale (min)
C_0	initial SVOC concentration in gas phase (μg m^{-3})
C_{gas}	SVOC concentration in gas phase (μg m^{-3})
C_{wall}	SVOC concentration on wall surface (μg m^{-3})
K_{eq}	gas-surface equilibrium constant
$C_{FEP\_surface}$	equivalent organic mass concentration of the FEP chamber surface (mg m^{-3})
M_{wall}	average molecular mass of the Teflon wall (g mol^{-1})
$\gamma_{FEP\_surface}$	activity coefficient in the Teflon surface
R	gas constant (J K^{-1} mol^{-1})
T	temperature (K)
$P_s(T)$	saturation vapor pressure of compound at temperature T (Pa)

406

407 **Figure 1.** Schematic diagram of the experimental setup.

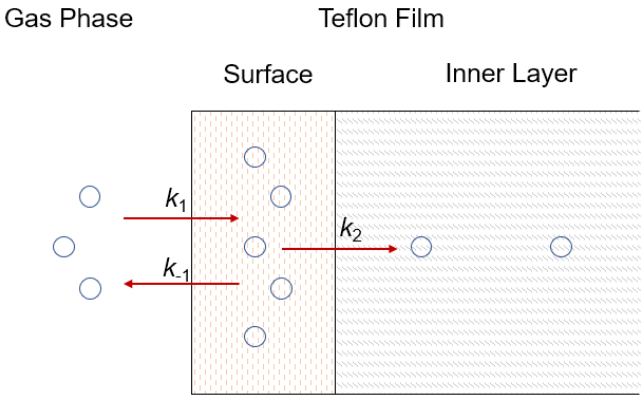

408

409 **Figure 2.** Schematic diagram of wall loss process. Compounds partition between gas phase and surface layer with forward
410 and backward rates (k_1 and k_{-1}). Compounds in surface layer undergo irreversible diffusion into inner layer with first-order
411 loss rate (k_2).

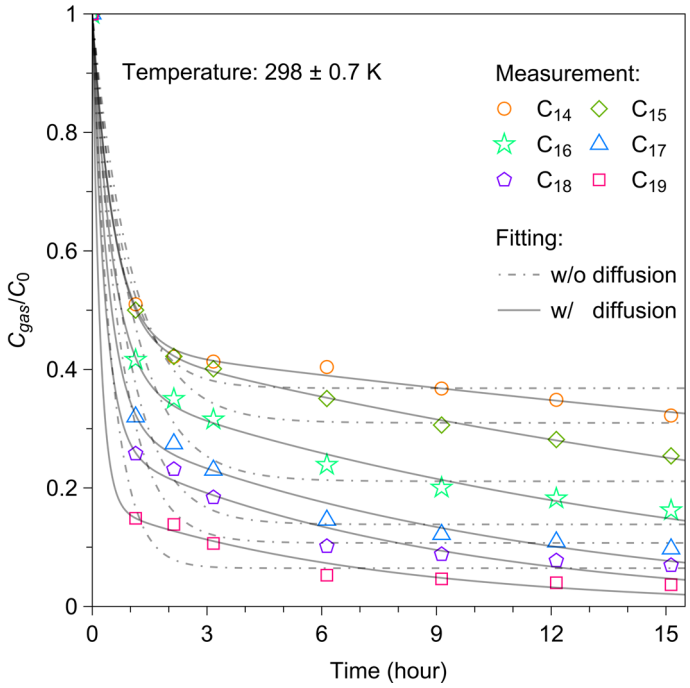

412

413 **Figure 3.** Temporal variation in C_{gas}/C_0 for C_{14}-C_{19} *n*-alkanes at 298 ± 0.7 K following injection. C_{gas} is the concentration of
414 each *n*-alkane in the gas phase, and C_0 is the corresponding initial concentration of each *n*-alkane. The two-layer kinetic
415 sorption model (Section 2.2) was employed to fit the data (black solid line). The black dot-dashed lines show the fitting result
416 to the model that ignores the diffusion process to the inner layer (*i.e.*, $k_2 = 0$).

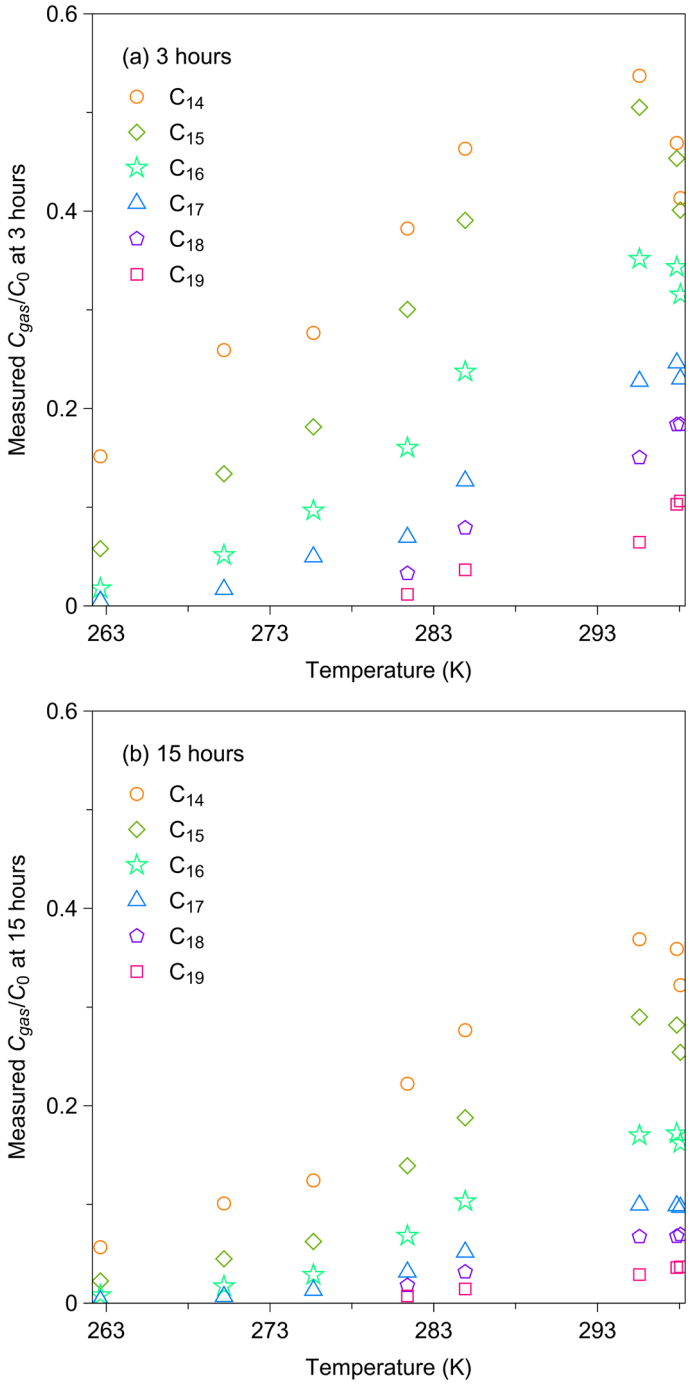

417

418 **Figure 4.** Measured values of C_{gas}/C_0 at (a) 3 hours and (b) 15 hours after injection.

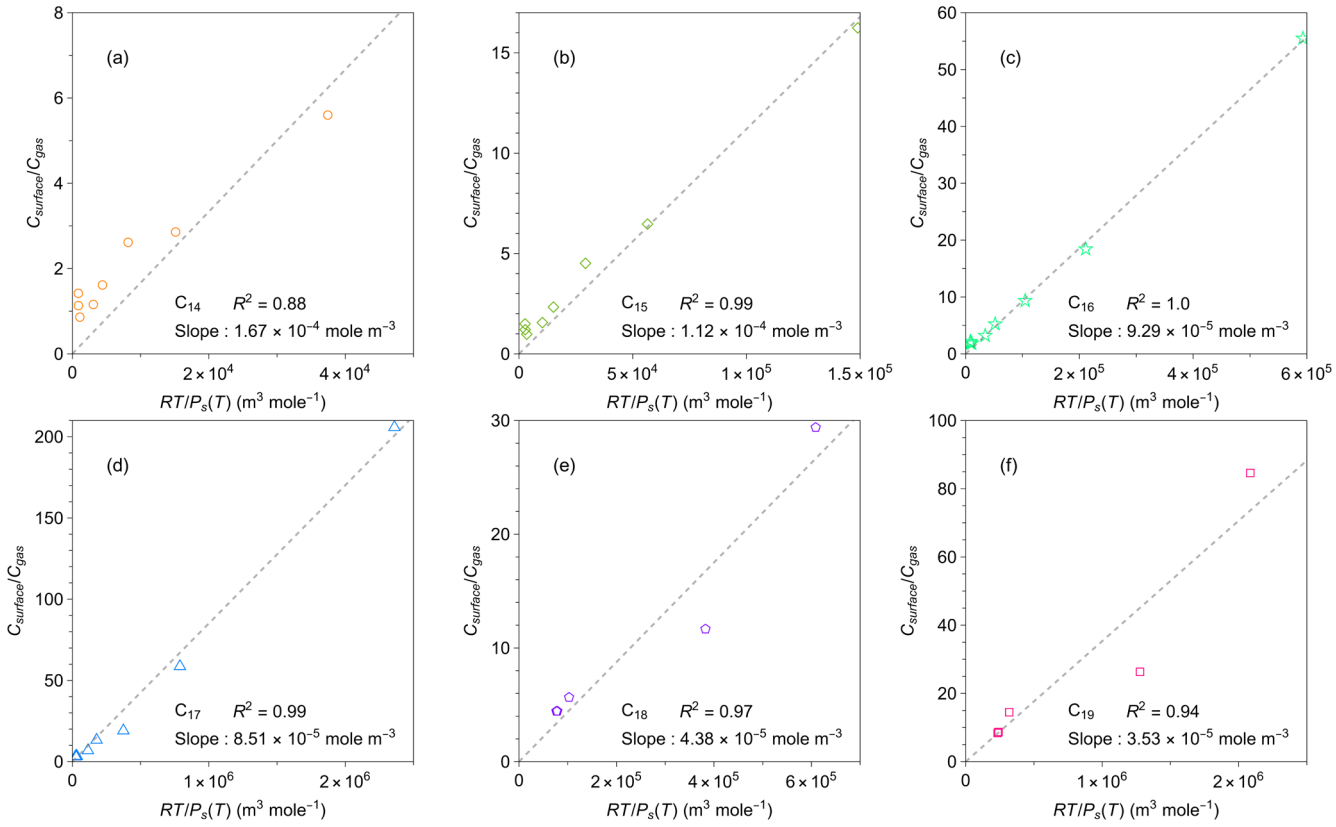

419

420 **Figure 5.** Relationships between measured ratio of concentrations in the chamber wall surface phase and in the gas phase at
421 quasi-equilibrium and calculated values of $RT/P_s(T)$ for individual *n*-alkanes. Calculation methods for $C_{surface}/C_{gas}$ is
422 detailed in the text. The values of $RT/P_s(T)$ for each *n*-alkane were calculated by the EVAPORATION group contribution
423 method (Compernolle et al., 2011). The black dashed lines are best linear fits of the data for each *n*-alkane.

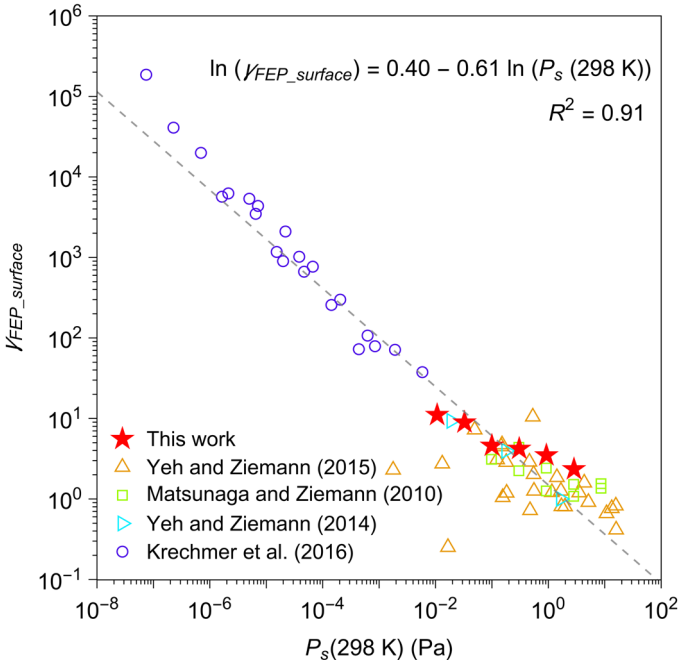

424

425 **Figure 6.** Activity coefficient ($\gamma_{FEP\_surface}$) of organic compounds in FEP film. The sources of data include this work and the
426 literature (compiled by Huang et al. (2018b), including Matsunaga and Ziemann (2010), Yeh and Ziemann (2014, 2015), and
427 Krechmer et al. (2016)). A list of chemical species that were investigated by each study is available in Table S4. Saturation
428 vapor pressures at 298 K (P_s(298 K)) were estimated by EVAPORATION (Compernolle et al., 2011).

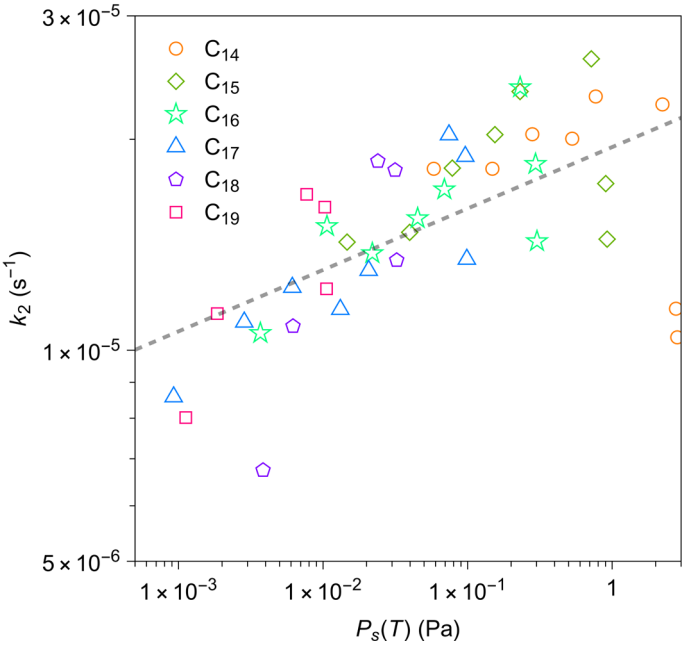

429

430 **Figure 7.** Relationship between calculated first-order loss rate k_2 for each *n*-alkane and calculated values of saturation vapor
431 pressure by the EVAPORATION group contribution method (Compernolle et al., 2011). The calculation method for k_2 is
432 detailed in the text. The black dashed line is the best linear fit to the data in a logarithmic scale.